Original Article
Identifying the characters of carotid plaques by gemstone spectral imaging and pathologic correlation

Xue-Jun Liu[1], Jian-Hong Wang[2], Peng Zhang[1], Wei-Wei Fu[3], Shi-Fang Li[4], Qing-Lan Sui[1], Wen-Jian Xu[1]

Departments of [1]Radiology, [3]Pathology, [4]Neurosurgery, The Affiliated Hospital of Qingdao University, Qingdao 266003, China; [2]The Organ Transplantation Center, The Affiliated Hospital of Qingdao University, Qingdao 266003, China

Abstract: Objective: To investigate the identification on the characters and analysis on the tissues of the carotid plaques in patients with carotid atherosclerosis (CAS) by gemstone spectral imaging (GSI). Methods: 42 patients were diagnosed as CAS by color doppler ultrasound. 20 of them were with carotid endarterectomy (CEA), as the control group (group B). The plaques of the 20 patients were resected and identified by pathological analysis. The 22 without CEA were in the group A. All the patients were received computed tomography angiography (CTA). The quality control (QC) images (140 Kvp) and the 80 kev single energy images were collected and transferred to the GE workstation AW4.4. The contrast to noise ratio (CNR) of the two were calculated and compared. The spectral HU curves were reconstructed and the effects on different kinds of plaque were evaluated according to the sensitivity and specificity of the curve slop, the iodine concentration (100 μg/mL) and the Effective-Z. Results: The average CNRs with 80 kev of the two groups were higher than with the QC images, significantly (P<0.01). The sensitivity and specificity of spectral HU curve slop on fibrous plaques were higher, comparing with other plaques, while the sensitivity was lowest and the specificity was the highest on lipid plaques. The sensitivity and specificity of both the iodine concentration and Effective-Z on the three kinds of plaque were lower than the slope of the curve. Conclusions: GSI was the reliable method to analyze and type on plaques. Using the CNR with 80 kev to determine the characters of the plaques was more suitable than with QC images. Spectral HU curve slope was the effective and credible index to evaluate different kinds of plaque.

Keywords: Atherosclerosis, gemstone spectral imaging, vulnerable plaque, case-control

Introduction

Cerebrovascular disease, as the systemic disease [1], was one of the three major causes of human death, 70% were the ischemic cerebrovascular disease. Atherosclerosis (AS) was the important factor causing cerebrovascular disease, which induced cerebral infarction, coronary disease and so on, while carotid atherosclerosis (CAS) was the major factor leading to cerebral ischemia. The major potential pathogenesis was due to the vulnerable plaque (VP) [2, 3], as the unstable plaques and with the tendency to thrombosis, including lipid plaques, fibrous plaques and mixed plaques [4, 5]. The destruction of VP by physical methods would induce acute myocardial infarction of the patients with AS [6]. Therefore, the investigations on the symptoms or characteristics of VP were

helpful to the diagnosis, prevention and treatment of AS [7, 8].

Clinically, most of the patients with AS were checked and analyzed by the methods of angiography and relative technologies, such as intravascular ultrasound (IVUS), angioscope, multi-detector computed tomography angiography (MDCT), intravascular magnetic resonance imaging (IMRA), magnetic resonance imaging (MRI), intravascular optical coherence tomography (IVOCT), positro emission tomography (PET) and so on [8-10].

Comparing to the traditional CT with lower sensitivity and specificity, gemstone spectral imaging (GSI) was the newly functional imaging technology, which could achieve the switching of two different kinds of energy in one period of

Table 1. The number and distribution of the plaques in group A and group B

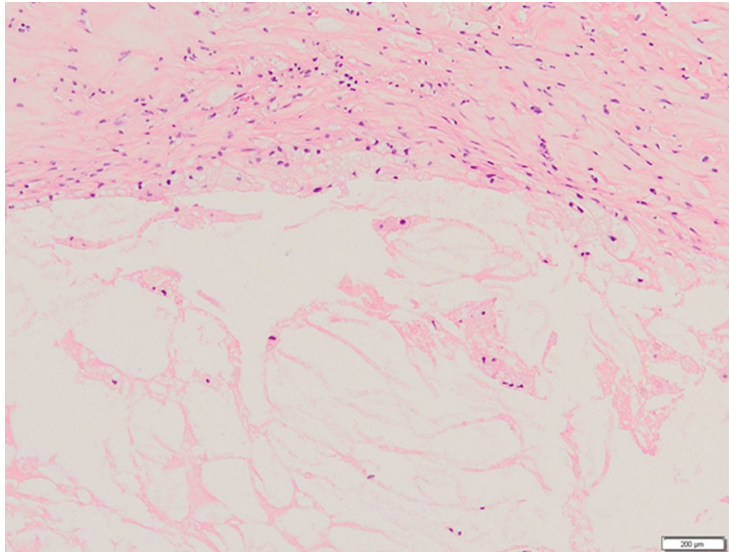|	Group A	Group B
Left common carotid artery	9	0
Left internal carotid artery	6	0
The furcation of left common carotid artery	11	9
Right common carotid artery	10	0
Right internal carotid artery	4	0
The furcation of right common carotid artery	13	11

Figure 1. Lipid plaque (100×): foam cells around the sphacelus and myofibroblast proliferation.
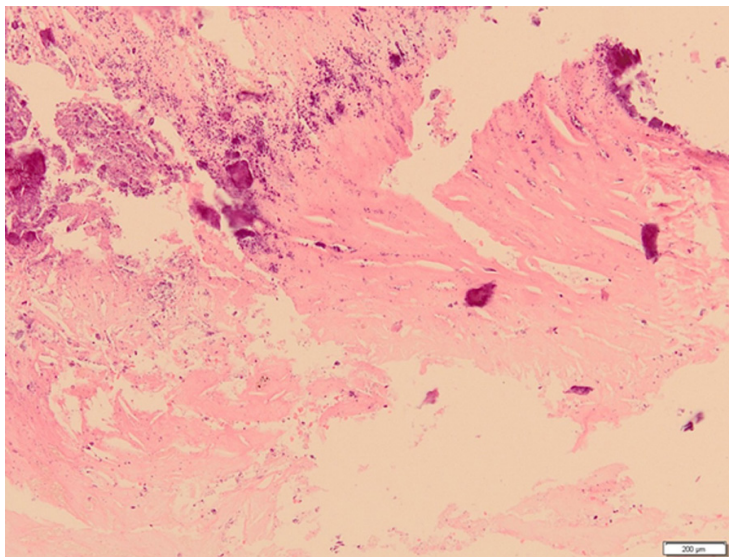

Figure 2. Fibrous plaque (100×): cholesterol crystal and calcification in the sphacelus.

spinning, then the different data were collected at the same time and the same angle, almost [11-13]. According to the different absorption coefficient of different substances under differently single energy, the attenuation images could be obtained and the substances could be separated then generated the new substances with images including water, calcium and iodine [14].

In our study, we used GSI to analyze and identify the lipid plaques, fibrous plaques and mixed plaques in CAS, and then selected the suitable index to evaluate different kinds of plaque.

Materials and methods

Equipment

GE Discovery CT750 HD and GE LOGIQ E9 were obtained from Ling Zeng Trading Co., Ltd. Shanghai, China. Leica RM2245 slicer, Leica ASP6025 automation tissue dehydrating machine and Leica EG1150H embedded system were obtained from Leica Biosystems, Beijing, China. Leica DM4P microscopy was obtained from Leica Microsystems, Beijing, China. -80°C refrigerator was obtained from Beijing AochuangXingye Technology Development Co., Ltd. China. High-speed centrifugation was obtained from Thermo Fisher Scientific Inc. Shanghai, China. TGL 16 K low-speed centrifugation was obtained from ZhuHai HEMA Medical Instrument Co., Ltd. Zhuhai, China. AB-160 electronic analytical balance was obtained from Denver, Shanghai Wanning Precision Scientific Instruments Co. Ltd. (China). PH Meter was obtained from Shanghai REX
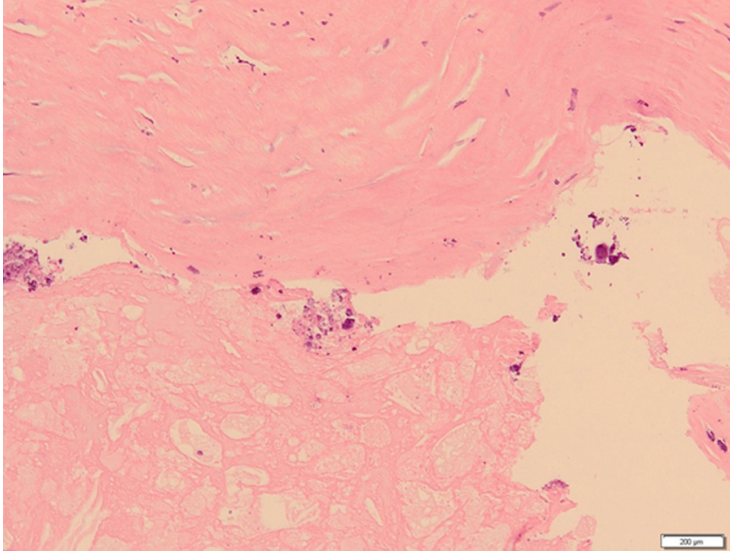
Figure 3. Mixed plaque (100×): Atherosclerotic sphacelus was showed below.

Instrument Factory, Shanghai, China. High pressure sterilizer was obtained from Hirayama, HUAYUE Inc. Guangzhou, China. Milli-Q ultrapure water system was obtained from Merck Millipore Corporation. Shanghai, China.

Agents

Iohexol (350 mgI/ml) was obtained from BEILU Pharmaceutical Co., Ltd. Beijing, China. 10% formalin and EDTA decalcifying solution were obtained from Qingdao Jie Shi Kang Biotechnology Co., Ltd. Qingdao, China. Paraffin, xylene, ethanol, hematoxylin, hydrochloride (HCl) and eosin were obtained from Bogoo Biotechnology Co., Ltd. Shanghai, China.

Patients and groups

42 patients, 26 male and 16 female, age 41 to 75, median age 63±3.5, were diagnosed as CAS in the Affiliated Hospital of Qingdao University (Qingdao, China) from January 2012 to December 2014. The included criteria were followed: 1. without the history of carotid artery stenting or CEA; 2. with obviously unilateral or bilateral carotid stenosis (luminal stenosis > 50%) by color doppler ultrasound; 3. with the capacity to receive carotid CT angiography by GSI; 4. at least one noncalcified plaque with the thickness more than 3 mm and 3 continuously visible aspects by the checking with GSI.

The excluded criteria were followed: 1. with the contraindications of CT scan including metal implantation, claustrophobia and so on; 2. with stroke at acute period and unstable situation, unconsciousness, intolerance or rejecting examination; 3. without informed consent; 4. rejecting surgical treatment.

The 42 patients were divided into group A (22 cases) and group B (20 cases), randomly.

CEA and pathological analysis

In the 42 patients, 20 of them (group B) were received CEA in the following week after CT scan. The patients were with percent stenosis above 70% and obvious symptoms of cerebral ischemia but not obvious remission after drug therapy. The CEA was taken by the neurovascular surgeon with more than 20 years experiences and the plaques were completely resected as the whole. The plaques were identified by pathological analysis, finally completed and obtained consistency by two pathologic doctors, blindly. The plaques were fixed with 10% formalin without collapse and destruction, then decalcified and cut into cubes of 3 mm^3. After fixed with paraffin, the cubes were made into slices of 5 μm and stained with hematoxylin-eosin (HE staining). The slices were observed under microscopy.

According to the classification standard of American Heart Association (AHA), the plaques were characterized as the lipid plaque, fibrous plaque and mixed plaque.

CT imaging examination

42 patients were scanned by color doppler ultrasound with GE LOGIQ E9 to determine whether there were obviously unilateral or bilateral carotid stenosis (luminal stenosis >50%) or atherosclerotic plaques forming. The examination before CEA was carried with GE Discovery HD 750 from the arch of aorta to the Willis circle of the cerebral artery. The contrast agent, iohexol (350 mgI/ml), was intravenously injected with the speed of 4.0 ml/s and the volume of 60 ml. 40 ml of saline was injected followed by
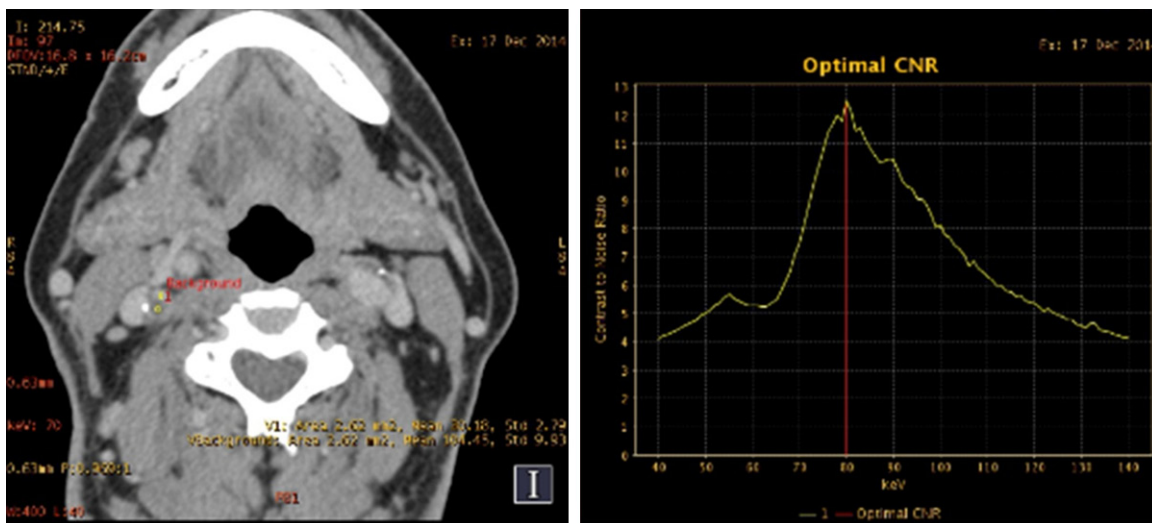
Figure 4. CNR with 80 kev: ROI was placed on the plaque and the Optimal CNR image was obtained on the right.

Table 2. The data of the images in group A and group B with optimal-CNR model

	Group A (n=53)	Group B (n=20)	P value
The best kev value (kev)	64~76	60~77	>0.05
Average of the best kev value (kev)	72.23±2.56	74.19±3.41	>0.05
CNR of the 80 kev value	36.75±5.56	35.77±4.46	>0.05
CNR of the QC image	28.67±2.23*	29.95±4.45**	>0.05
P value	<0.05	<0.05	

Note: *comparing to the CNR of the 80 kev value in group A; **comparing to the CNR of the 80 kev value in group B.

iohexol. The region of interest (ROI) was located on the center of the aortic arch. The concentration of iohexol was traced with Smart Prep software with 100 Hu threshold value. The scan was carried automatically 5 seconds after reaching 100 Hu with the model of GIS (tube voltage with transient switching between 80 keV and 140 keV, tube current of 600 mA, rotation time of 0.5 s, coverage area of the detector of 40 mm, matrix of 512×512, slice thickness of 0.625 mm, interlayer distance of 0.625 mm, pitch of 0.984:1. The QC (140 Kvp mixed energy) and 80 kev single energy images were obtained with thickness of 0.625 mm and interlayer distance of 1.25 mm.

Images and data collecting

The 80 kev images were sent to the GE energy spectrum CT workstation AW4.4. By the GSI-view technology and the optimal-CNR model, took the maximum cross section of the plaques with the ROI being placed in the plaques and the adjacent artery lumen, then the CT values (CT_1, CT_0) and SD values (SD_1, SD_0) were measured. The ROI of the plaque was taken as 2 mm^2, while the artery ROI was taken as 3 mm^2. The best kev values (80 kev) of the contrast to noise ration (CNR) in different plaques were obtained. The CNR values with the QC images and the 80 kev were calculated according to $CNR = (|ROI_1 - ROI_0|)/(SD_1^2 + SD_0^2)^{1/2}$ and the differences were compared.

GSI analysis

The spectrum curve slop, the iodine concentration (100 μg/mL) and the Effective-Z under the QC images and 80 kev in the two groups were obtained. The density values of the plaques were calculated with the thickness over than 3 mm and the ROI of 2 mm^2. The average value of the measurements was calculated, totally 3 times. In order to reduce the influence including the iohexol, the fat and the calcification artifacts on the measurements, the slice concordance was on the minimal lumen stenosis avoiding the adjacent lumen, adipose tissues and calcification.

By Spectral-Curve analysis, the ROI of 1 mm^2 was taken on the minimal lumen stenosis of the carotid artery on the horizontal axial image, while the ROI of 1 mm^2 was placed on the adi-
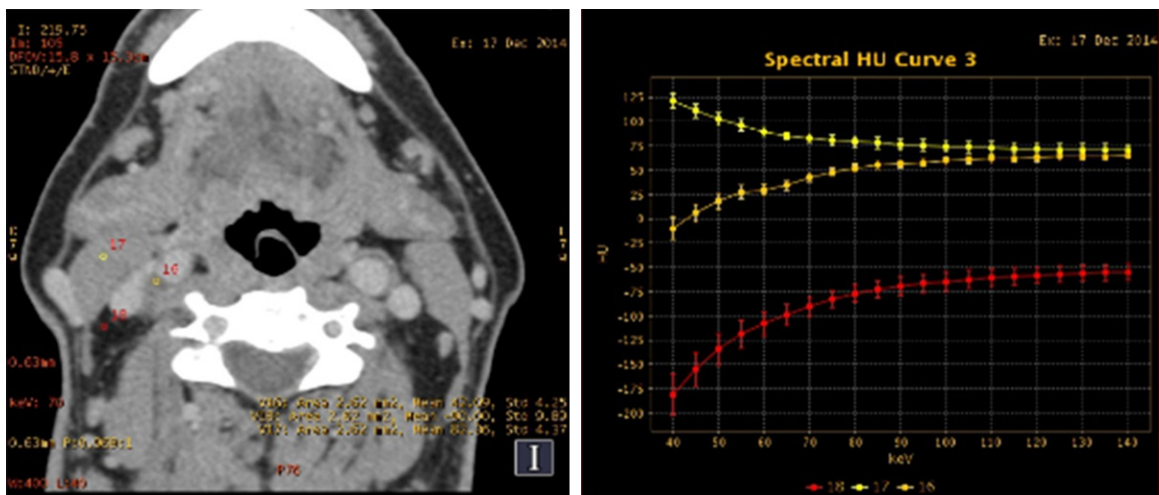
Figure 5. The spectrum curve of lipid plaque: ROI was placed on the plaque, fibrous and adipose tissues, and the spectrum curves were obtained on the right, 18 as adipose tissue, 17 as the fibrous tissue and 16 as the plaque. The plaque was identified as lipid plaque with the spectrum curve similar to the adipose tissue.
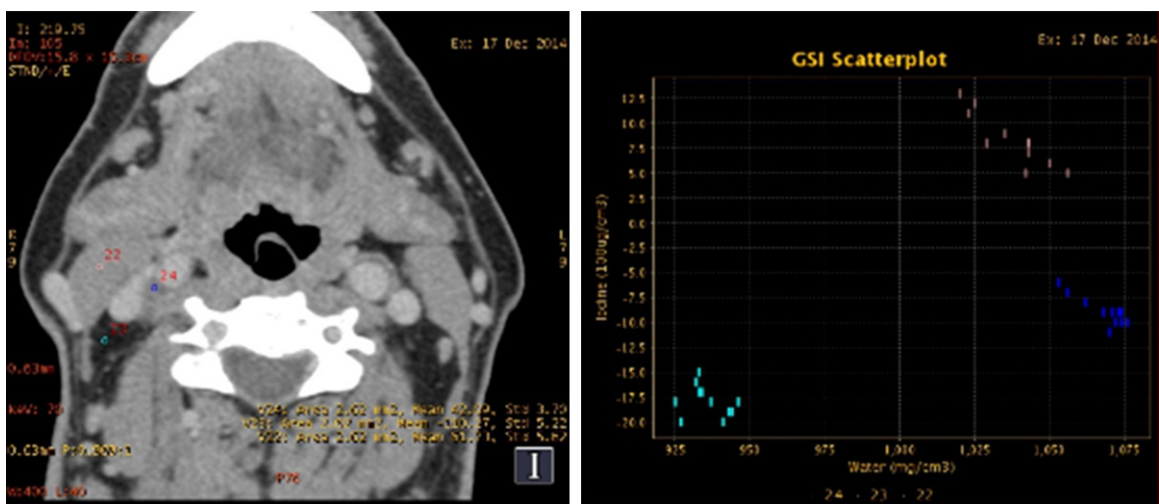

Figure 6. The iodine concentration image of lipid plaque: ROI was placed on the plaque, fibrous and adipose tissues, and the iodine concentration images were obtained on the right, 23 as adipose tissue, 22 as the fibrous tissue and 24 as the plaque.

pose and muscle tissues under the same level. The spectrum curves of the plaques, adipose and muscle tissues were obtained. Took the spectrum curves of the adipose and muscle tissues as the reference standards. The spectrum curve of the plaque closed to the adipose tissue indicated the lipid plaque (convex type), while the one closed to the muscle tissues was the fibrous plaque. The curve between the two indicated the mixed plaque. Calculated the curve slope according to $K=(CT_a-CT_b)/(Kev_a-Kev_b)$. In our study, we took the CT values of 40 kev and 110 kev, then the curve slope was calculated according to $K=(CT_a-CT_b)/80$.

Basing on the images of the substance concentration, measured the iodine concentration (100 µg/ml) of the plaque ROI and the aspect of the plaque in the artery lumen, separately. Calculated the normalized iodine concentration (NIC) of the plaque ROI, the ratio of the iodine concentration between the plaque ROI and the artery lumen, and obtained the average value, totally 3 times.

Basing on the images of the Effective-Z, measured the effective atomic number of plaque ROI and obtained the average value, totally 3 times.
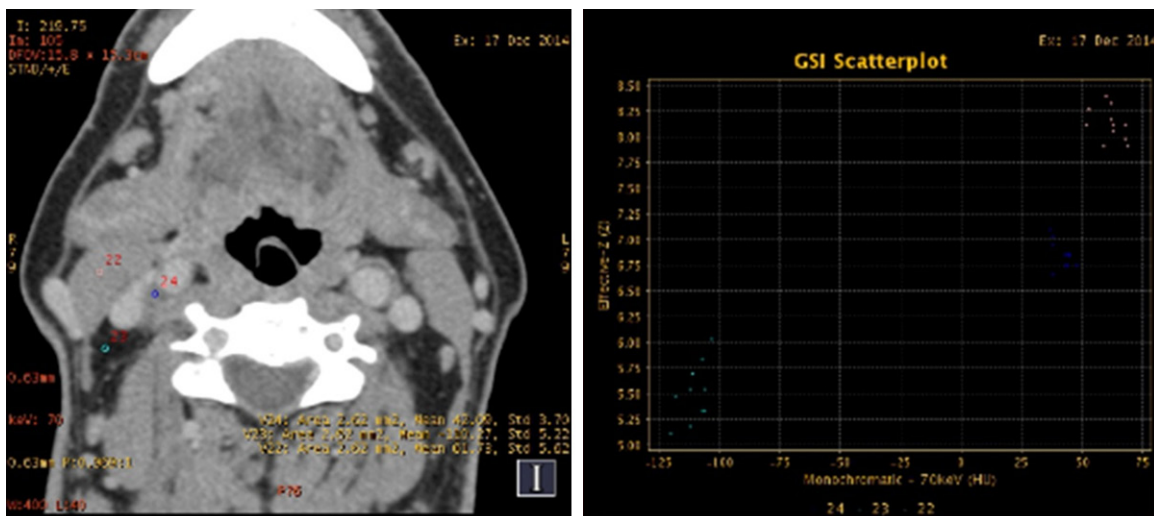
Figure 7. The Effective-Z image of lipid plaque: ROI was placed on the plaque, fibrous and adipose tissues, and the Effective-Z image were obtained on the right, 23 as adipose tissue, 22 as the fibrous tissue and 24 as the plaque.
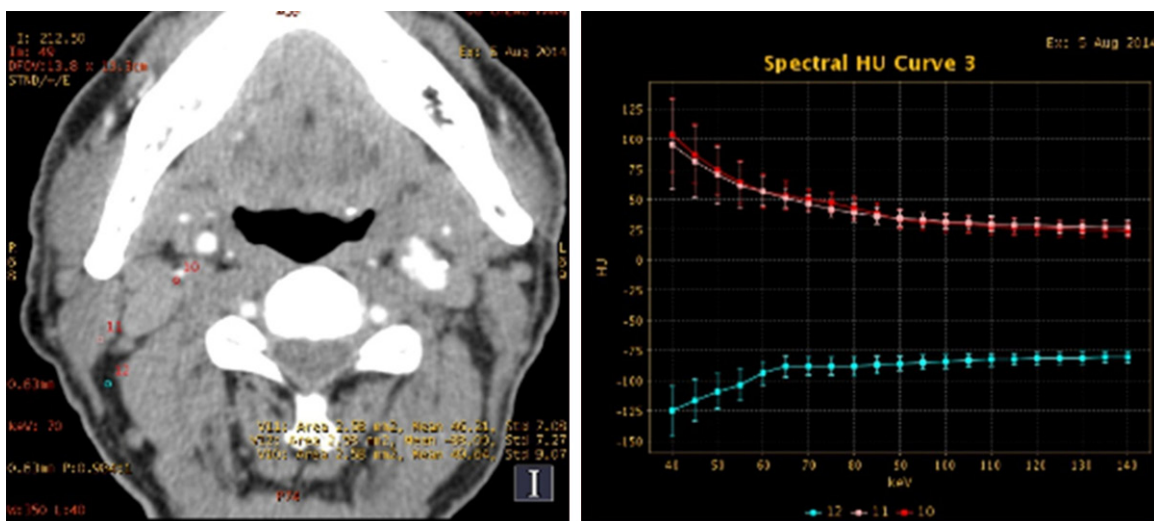

Figure 8. The spectrum curve of fibrous plaque: ROI was placed on the plaque, fibrous and adipose tissues, and the spectrum curves were obtained on the right, 12 as adipose tissue, 11 as the fibrous tissue and 10 as the plaque. The plaque was identified as fibrous plaque with the spectrum curve similar to the fibrous tissue.

The plaques density under the QC images and 80 kev in the two groups were measured and the differences were compared.

Statistical analysis

All the data were analyzed with SPSS 19.0 software and presented as mean ± standard deviations (X±SDs). Independent *t*-test was used to analyze the CNR values of plaque ROI under QC images and 80 kev in the two groups. A value of $P<0.05$ considered significant difference. The ROC curves of the slope, iodine concentration and Effective-Z to the three kinds of plaque including lipid plaque, fibrous plaque and mixed plaque were obtained. The maximal combined value of the sensitivity and the specificity was taken as the best diagnostic threshold value. Evaluated the diagnostic effects of the curve slope, iodine concentration and Effective-Z on different kinds of plaque.

Results

Plaques and distribution

There were 86 plaques checked by CTA in the 42 patients, while 65 out of the 86 were includ-
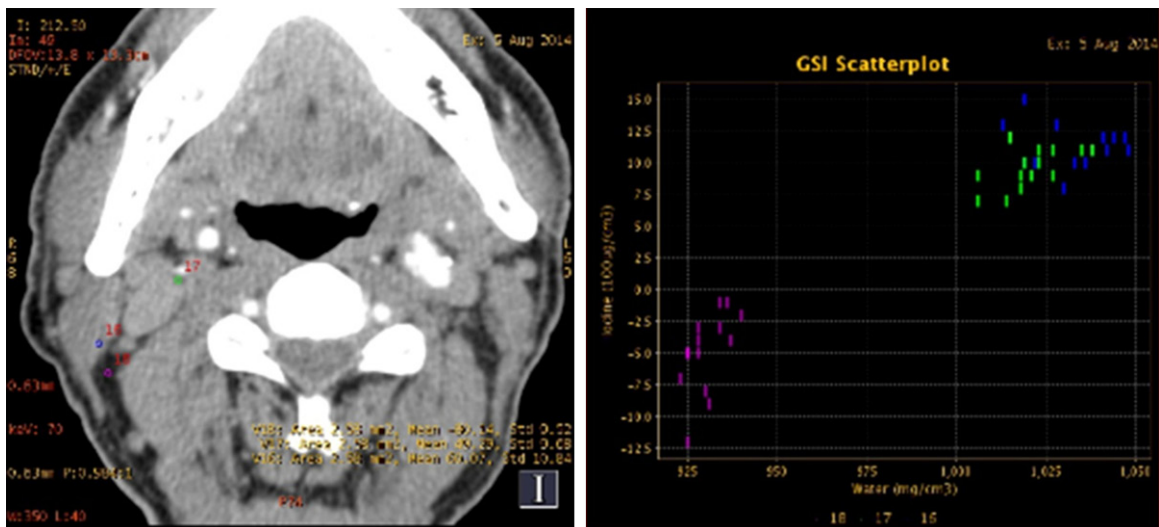
Figure 9. The iodine concentration image of fibrous plaque: ROI was placed on the plaque, fibrous and adipose tissues, and the iodine concentration images were obtained on the right, 18 as adipose tissue, 16 as the fibrous tissue and 17 as the plaque.
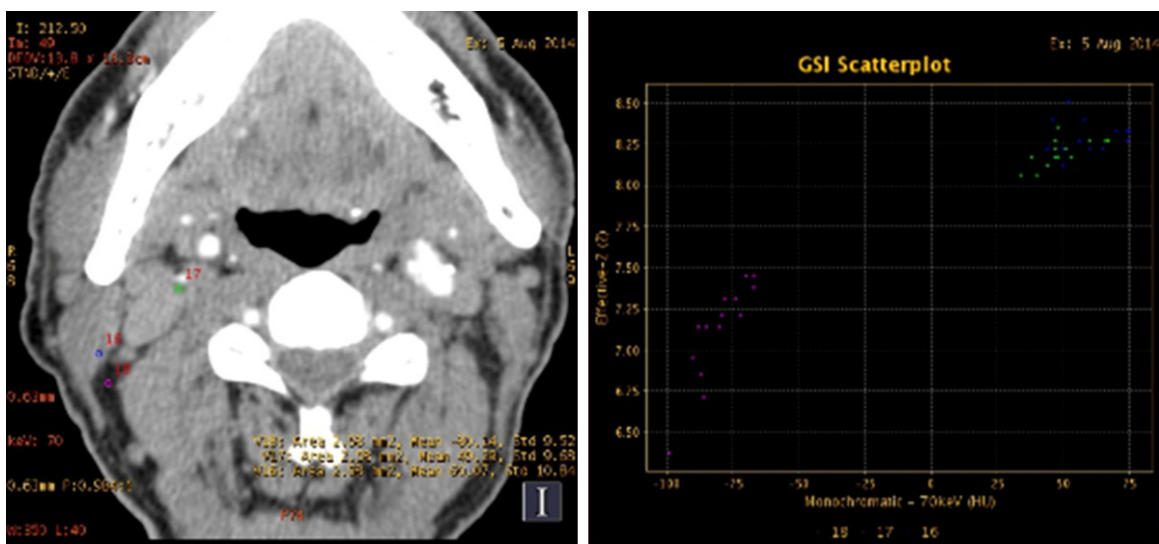

Figure 10. The Effective-Z image of fibrous plaque: ROI was placed on the plaque, fibrous and adipose tissues, and the Effective-Z image were obtained on the right, 18 as adipose tissue, 16 as the fibrous tissue and 17 as the plaque.

ed, 53 in group A, 20 in group B. The number and distributions of the plaques were showed in **Table 1**.

Histopathological analysis

According to the classification standard of American Heart Association (AHA), there were 7 lipid plaques as type IV (thin fibrous cap and necrotic lipoid nucleus), 9 fibrous plaques as type V and type VIII (not obvious lipoid nucleus) and 4 mixed plaques as type VI (fibrous tissue and lipoid nucleus). The histopathological characteristics of the plaques were showed in **Figures 1**-**3**.

Images of the best kev value and the relative data

The CNR (80 kev) image with the ROI being on the plaque was showed in **Figure 4**.
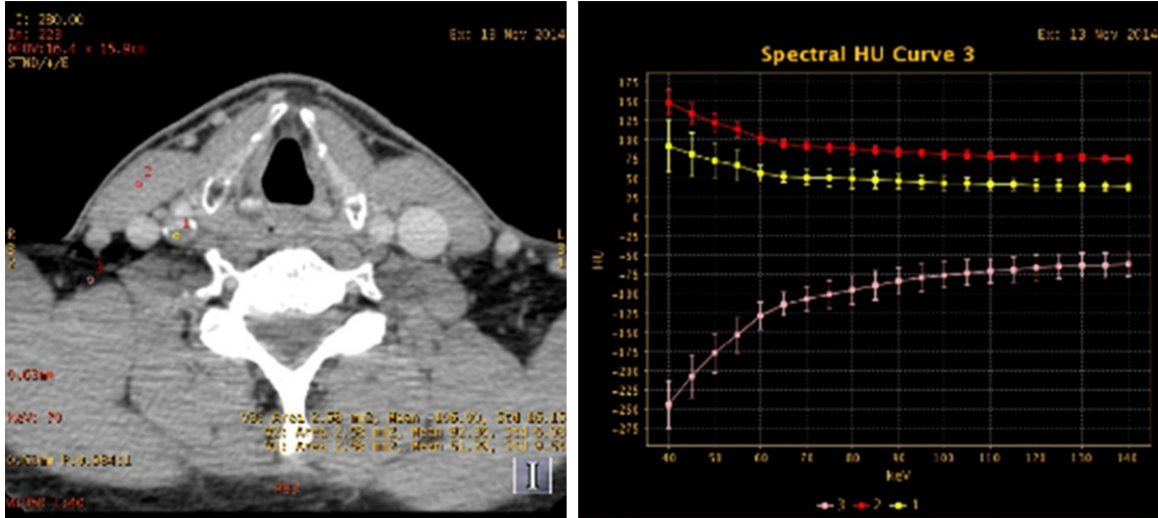
Figure 11. The spectrum curve of mixed plaque: ROI was placed on the plaque, fibrous and adipose tissues, and the spectrum curves were obtained on the right, 3 as adipose tissue, 2 as the fibrous tissue and 1 as the plaque. The plaque was identified as mixed plaque with the spectrum curve between the fibrous and adipose tissues.
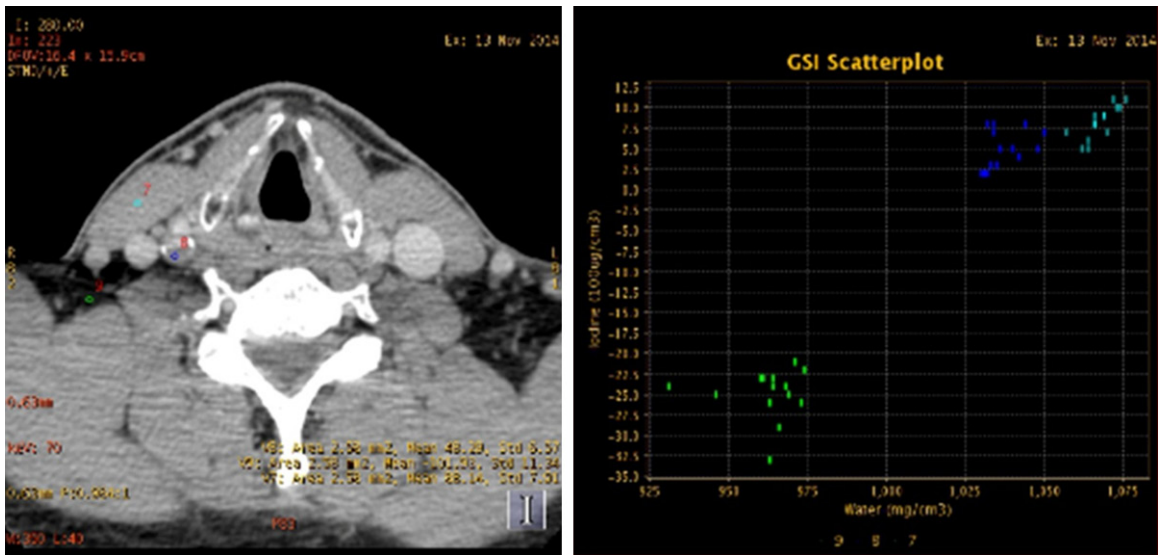

Figure 12. The iodine concentration image of mixed plaque: ROI was placed on the plaque, fibrous and adipose tissues, and the iodine concentration images were obtained on the right, 9 as adipose tissue, 7 as the fibrous tissue and 8 as the plaque.

With the optimal-CNR model, the data of the images in the two groups were showed in **Table 2**.

With the optimal-CNR model and the data in **Table 2**, there were no significant differences of the best kev values, CNR of the 80 kev and CNR of the QC images between the two groups. However, there were significant differences between the average CNR with 80 kev and the average CNR with QC images in the two groups, separately (*P*<0.05).

Images of the spectrum curve, iodine concentration and Effective-Z

In group A, there were 53 plaques including 11 lipid plaques (A1), 20 fibrous plaques (A2) and 22 mixed plaques (A3). In group B, there were 20 plaques including 7 lipid plaques (B1), 9 fibrous plaques (B2) and 4 mixed plaques (B3).
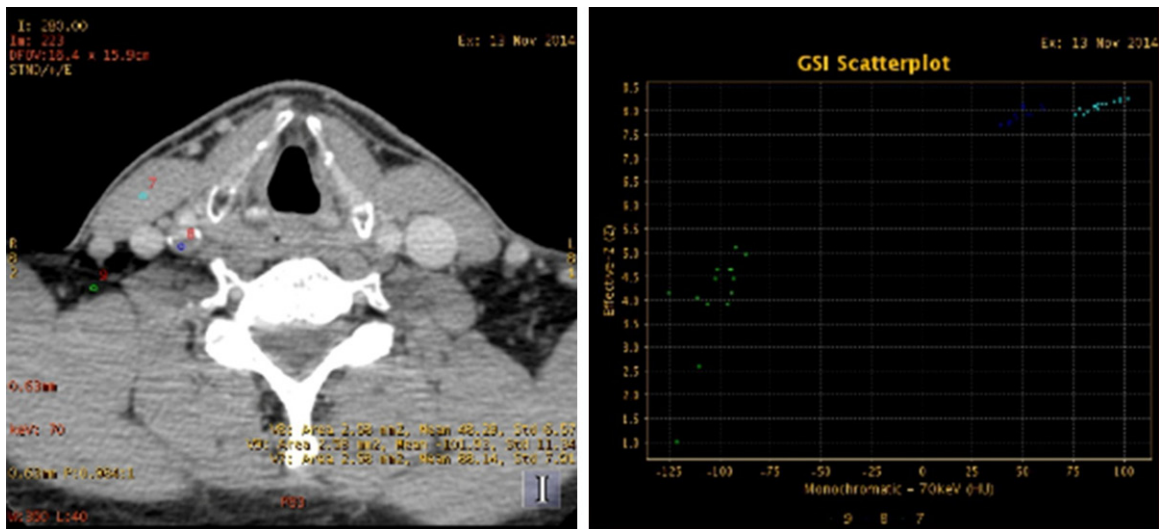
Figure 13. The Effective-Z image of mixed plaque: ROI was placed on the plaque, fibrous and adipose tissues, and the Effective-Z image were obtained on the right, 9 as adipose tissue, 7 as the fibrous tissue and 8 as the plaque.
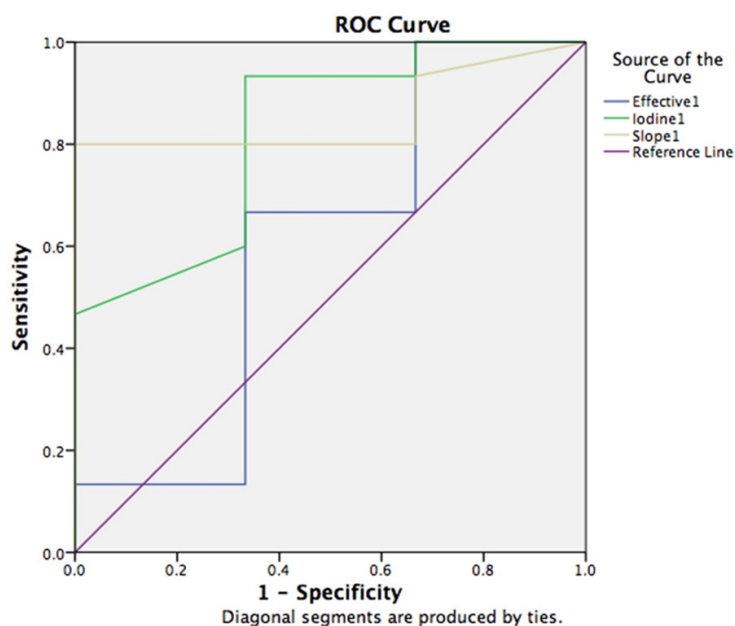

Figure 14. ROC curve of the curve slope, iodine concentration and Effective-Z on the lipid plaque.

The spectrum curve, iodine concentration and Effective-Z of lipid plaque: With lipid plaque, the image of the spectrum curve was showed in **Figure 5**, the iodine concentration showed in **Figure 6** and the Effective-Z showed in **Figure 7**.

The spectrum curve, iodine concentration and Effective-Z of fibrous plaque: With fibrous plaque, the image of the spectrum curve was showed in **Figure 8**, the iodine concentration showed in **Figure 9** and the Effective-Z showed in **Figure 10**.

The spectrum curve, iodine concentration and Effective-Z of mixed plaque: With mixed plaque, the image of the spectrum curve was showed in **Figure 11**, the iodine concentration showed in **Figure 12** and the Effective-Z showed in **Figure 13**.

ROC curves

ROC curves: The ROC curves including the curve slope, iodine concentration and Effective-Z on the lipid plaque was showed in **Figure 14** and **Table 3**, the fibrous plaque in **Figure 15** and **Table 4**, and the mixed plaque in **Figure 16** and **Table 5**.

Diagnosis on plaques: According to parameters showed in **Table 6**, the sensitivity (75.6) of curve slope was higher but the specificity (80.9) was lower on the fibrous plaque comparing with mixed plaque, while the highest specificity (94.0) and the lowest sensitivity (54.4) on the lipid plaque. The specificity and sensitivity of iodine concentration and Effective-Z on the 3 kinds of plaque were lower, comparing to the curve slope.

Discussions

AS, as the complicatedly synthetic process, mostly happened in carotid artery, aorta, coronary

Table 3. Area under the curve of the ROC curve including the curve slope, iodine concentration and Effective-Z on the lipid plaque

Area Under the Curve					
Test Result Variable (s)	Area	Std. Error[a]	Asymptotic Sig.[b]	Asymptotic 95% Confidence Interval	
				Lower Bound	Upper Bound
Effective1	.600	.217	.594	.175	1.000
Iodine1	.822	.136	.086	.556	1.000
Slope1	.856	.092	.058	.675	1.000

[a]Under the nonparametric assumption; [b]Null hypothesis: true area=0.5.
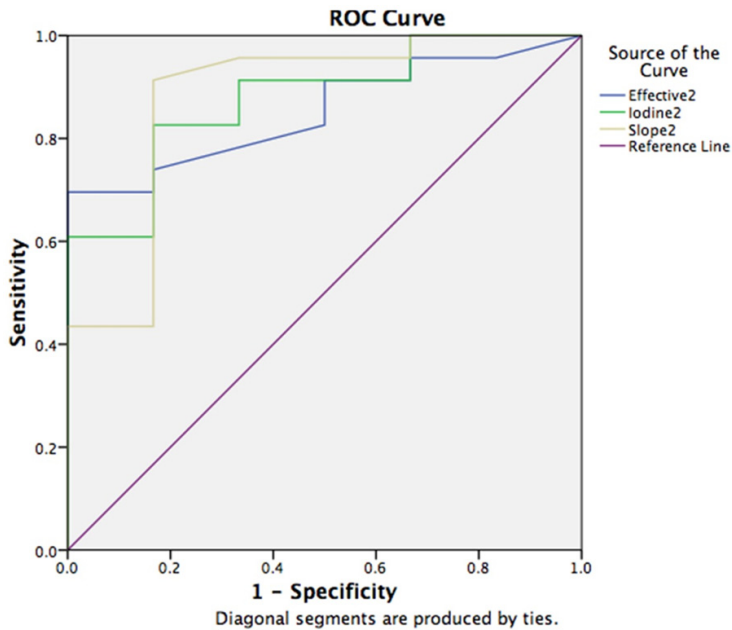

Figure 15. ROC curve of the curve slope, iodine concentration and Effective-Z on the fibrous plaque.

Table 4. Area under the curve of the ROC curve including the curve slope, iodine concentration and Effective-Z on the fibrous plaque

Area Under the Curve					
Test Result Variable (s)	Area	Std. Error[a]	Asymptotic Sig.[b]	Asymptotic 95% Confidence Interval	
				Lower Bound	Upper Bound
Effective2	.851	.071	.009	.711	.992
Iodine2	.877	.071	.005	.737	1.000
Slope2	.880	.089	.005	.706	1.000

[a]Under the nonparametric assumption; [b]Null hypothesis: true area=0.5.

artery and peripheral arterial. CAS was common in elder people, the major cause inducing cerebral ischemia. The potential pathogenesis was due to breaking and dropping of the CAS plaques, the VP, inducing the embolism of cerebral circulation pathway [15, 16]. 87% of the cerebral infarction was ischemic cerebral infarction, while 20% of them were induced by CAS [17]. Previous studies [18-20] showed that the characteristics of the plaques decided their stability, which influenced the prognosis of the patients with cerebral infarction. Most of the plaques were not calcified, containing fiber and lipid. So, there were lipid plaque, fibrous plaque and mixed plaque. The unstable plaques, the VP, were with the morphologies of niche or surface irregularity, which were similar to wavy or crateriform [21].

From 1970s, more and more people received CEA to treat CAS [22], which was helpful to improve cerebral ischemia and reduce cerebral apoplexy. In our study, there were 42 patients with CAS diagnosed by CT scan, totally. 20 patients of them were successfully received CEA and the plaques were analyzed by pathological methods. Comparing to the 22 patients without CEA, we evaluated the analytical effects on the characteristics of different kinds of plaque by GSI technology.

GSI, as the newly energy spectrum imaging technology, improved the non-invasive complexity analysis on the CAS plaques clinically. By GSI, we comprehensively analyzed and evaluated the characteristics of the CAS plaques in the 42 patients. The CNR under QC image and 80 kev were obtained, separately. The results of the comparison showed that the average CNR of 80 kev in group A and group B were higher than of QC image, separately, which indicated that with the best kev, the evaluation on the characteristics of CAS plaques was more sensitive than with the QC image.
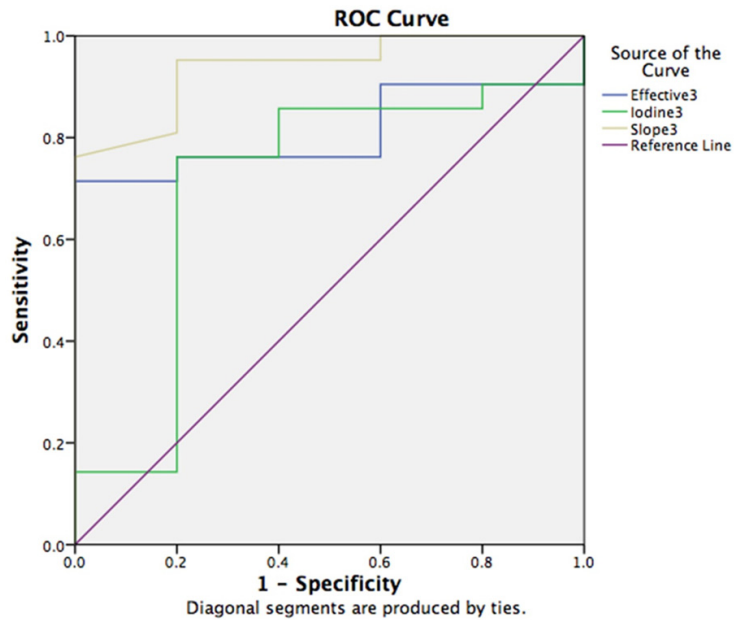
Figure 16. ROC curve of the curve slope, iodine concentration and Effective-Z on the mixed plaque.

Table 5. Area under the curve of the ROC curve including the curve slope, iodine concentration and Effective-Z on the mixed plaque

Test Result Variable (s)	Area	Std. Error[a]	Asymptotic Sig.[b]	Asymptotic 95% Confidence Interval	
				Lower Bound	Upper Bound
Effective3	.810	.083	.034	.646	.973
Iodine3	.705	.143	.162	.425	.985
Slope3	.938	.050	.003	.840	1.000

[a]Under the nonparametric assumption; [b]Null hypothesis: true area=0.5.

On the other hand, the images of spectrum curve slope, iodine concentration and Effective-Z were obtained. According to the ROC curves of the three mentioned above, we compared the sensitivity and specificity on lipid plaque, fibrous plaque and mixed plaque. We found that the curve slope was with higher sensitivity (75.6) but lower specificity (80.9) on fibrous plaque comparing to the mixed plaque, while with the highest specificity (94.0) and the lowest sensitivity (54.4) on the lipid plaque. But the specificity and sensitivity of iodine concentration and EffectiveZ on the 3 kinds of plaque were lower, comparing to the curve slope. Therefore, we considered the curve slope was more suitable to identify the different kinds of CAS plaques.

To draw a conclusion, in the detection of CAS plaques by GSI, the CT value with the best kev value and the spectrum curve slope were more suitable and credible.

However, due to the small samples and the limited scanning cases, there were influences on the results of evaluation. The CAS plaques in the 20 patients with CEA were identified by pathological analysis, as the control, while the 22 were without CEA. Depending on GSI and CT scan, the placements of ROI were with systematic deviation, artificially. All of these would have effects on the accuracy of the results. For example, the spectrum curve of the lipid plaque was convex type, similar to the lipoid tissue, but the average CT value, iodine concentration and Effective-Z presented as fibrous or mixed plaque, which might be caused by the accompanying blooding in the plaque. Due to the necrosis of the lipid plaque and the nourishing vessel on the core-periphery, there would be blooding in the plaque, then induced the increase of CT value, iodine concentration and Effective-Z closed to the fibrous and mixed plaques but with convex type. In the mixed plaque, there was inequality of size of necrotic cores and inhomogeneous of the whole density, which led to the differences of placements and sizes of ROI and the higher or lower CT value, iodine concentration and Effective-Z. The fibrous plaque was influenced less for the more homogeneous fibrous tissue.

The GSI is still in the research phases, and the quality of CT images is influenced by many factors, such as constructed defect [23]. The GSI has more advantages on the diagnosis of CAS and the evaluation on the characteristics of different kinds of plaque.

Table 6. Diagnosis on lipid plaque, fibrous plaque and mixed plaque by the spectral imaging parameters of CT arterial phase

Parameters	Plaques	Area under the curve	Threshold value	Sensitivity (%)	Specificity (%)
Curve slope	Lipid plaque	0.856	1.06	54.4	94.0
	Fibrous plaque	0.880	-10.6 µg/ml	75.6	80.9
	Mixed plaque	0.938	6.7	82.4	78.8
Iodine concentration	Lipid plaque	0.822	-1.07	93.7	89.6
	Fibrous plaque	0.877	8.3 µg/ml	76.7	77.6
	Mixed plaque	0.705	8.1	77.8	76.7
Effective-Z	Lipid plaque	0.600	-0.62	86.5	81.4
	Fibrous plaque	0.851	3.6 µg/ml	72.0	83.5
	Mixed plaque	0.810	7.7	76.9	70.6

Disclosure of conflict of interest

None.

Address correspondence to: Dr. Wen-Jian Xu, Department of Radiology, The Affiliated Hospital of Qingdao University, Qingdao 266003, China. Tel: +0532-82911004; Fax: +0532-82911004; E-mail: xuwenjian@vip.163.com

References

[1] Shinohara M, Yamashita T, Tawa H, Takeda M, Sasaki N, Takaya T, Toh R, Takeuchi A, Ohigashi T, Shinohara K, Kawashima S, Yokoyama M, Hirata K and Momose A. Atherosclerotic plaque imaging using phase-contrast X-ray computed tomography. Am J Physiol Heart Circ Physiol 2008; 294: H1094-100.

[2] Naghavi M, Libby P, Falk E, Casscells SW, Litovsky S, Rumberger J, Badimon JJ, Stefanadis C, Moreno P, Pasterkamp G, Fayad Z, Stone PH, Waxman S, Raggi P, Madjid M, Zarrabi A, Burke A, Yuan C, Fitzgerald PJ, Siscovick DS, de Korte CL, Aikawa M, Airaksinen KE, Assmann G, Becker CR, Chesebro JH, Farb A, Galis ZS, Jackson C, Jang IK, Koenig W, Lodder RA, March K, Demirovic J, Navab M, Priori SG, Rekhter MD, Bahr R, Grundy SM, Mehran R, Colombo A, Boerwinkle E, Ballantyne C, Insull W Jr, Schwartz RS, Vogel R, Serruys PW, Hansson GK, Faxon DP, Kaul S, Drexler H, Greenland P, Muller JE, Virmani R, Ridker PM, Zipes DP, Shah PK and Willerson JT. From vulnerable plaque to vulnerable patient: a call for new definitions and risk assessment strategies: Part II. Circulation 2003; 108: 1772-1778.

[3] Naghavi M, Libby P, Falk E, Casscells SW, Litovsky S, Rumberger J, Badimon JJ, Stefanadis C, Moreno P, Pasterkamp G, Fayad Z, Stone PH, Waxman S, Raggi P, Madjid M, Zarrabi A, Burke A, Yuan C, Fitzgerald PJ, Siscovick DS, de Korte CL, Aikawa M, Juhani Airaksinen KE, Assmann G, Becker CR, Chesebro JH, Farb A, Galis ZS, Jackson C, Jang IK, Koenig W, Lodder RA, March K, Demirovic J, Navab M, Priori SG, Rekhter MD, Bahr R, Grundy SM, Mehran R, Colombo A, Boerwinkle E, Ballantyne C, Insull W Jr, Schwartz RS, Vogel R, Serruys PW, Hansson GK, Faxon DP, Kaul S, Drexler H, Greenland P, Muller JE, Virmani R, Ridker PM, Zipes DP, Shah PK and Willerson JT. From vulnerable plaque to vulnerable patient: a call for new definitions and risk assessment strategies: Part I. Circulation 2003; 108: 1664-1672.

[4] Adiguzel E, Ahmad PJ, Franco C and Bendeck MP. Collagens in the progression and complications of atherosclerosis. Vasc Med 2009; 14: 73-89.

[5] Virmani R, Kolodgie FD, Burke AP, Farb A and Schwartz SM. Lessons from sudden coronary death: a comprehensive morphological classification scheme for atherosclerotic lesions. Arterioscler Thromb Vasc Biol 2000; 20: 1262-1275.

[6] Davies MJ. Stability and instability: two faces of coronary atherosclerosis. The Paul Dudley White Lecture 1995. Circulation 1996; 94: 2013-2020.

[7] Vukadinovic D, van Walsum T, Manniesing R, Rozie S, Hameeteman R, de Weert TT, van der Lugt A and Niessen WJ. Segmentation of the outer vessel wall of the common carotid artery in CTA. IEEE Trans Med Imaging 2010; 29: 65-76.

[8] Enterline DS and Kapoor G. A practical approach to CT angiography of the neck and brain. Tech Vasc Interv Radiol 2006; 9: 192-204.

[9] de Weert TT, de Monye C, Meijering E, Booij R, Niessen WJ, Dippel DW and van der Lugt A. As-

sessment of atherosclerotic carotid plaque volume with multidetector computed tomography angiography. Int J Cardiovasc Imaging 2008; 24: 751-759.

[10] Randoux B, Marro B, Koskas F, Duyme M, Sahel M, Zouaoui A and Marsault C. Carotid artery stenosis: prospective comparison of CT, three-dimensional gadolinium-enhanced MR, and conventional angiography. Radiology 2001; 220: 179-85.

[11] Lin XZ, Miao F, Li JY, Dong HP, Shen Y and Chen KM. High-definition CT Gemstone spectral imaging of the brain: initial results of selecting optimal monochromatic image for beam-hardening artifacts and image noise reduction. J Comput Assist Tomogr 2011; 35: 294-297.

[12] Zhang D, Li X and Liu B. Objective characterization of GE discovery CT750 HD scanner: gemstone spectral imaging mode. Med Phys 2011; 38: 1178-1188.

[13] Deng K, Zhang CQ, Li W, Wang JJ, Wang XY, Pang T, Wang GL and Liu C. Preliminary application of high-definition CT Gemstone Spectral Imaging in hand and foot tendons. Korean J Radiol 2012; 13: 743-751.

[14] Fletcher JG, Takahashi N, Hartman R, Guimaraes L, Huprich JE, Hough DM, Yu L and McCollough CH. Dual-energy and dual-source CT: is there a role in the abdomen and pelvis? Radiol Clin North Am 2009; 47: 41-57.

[15] Kondos GT, Hoff JA, Sevrukov A, Daviglus ML, Garside DB, Devries SS, Chomka EV and Liu K. Electron-beam tomography coronary artery calcium and cardiac events: a 37-month follow-up of 5635 initially asymptomatic low- to intermediate-risk adults. Circulation 2003; 107: 2571-2576.

[16] Vengrenyuk Y, Carlier S, Xanthos S, Cardoso L, Ganatos P, Virmani R, Einav S, Gilchrist L and Weinbaum S. A hypothesis for vulnerable plaque rupture due to stress-induced debonding around cellular microcalcifications in thin fibrous caps. Proc Natl Acad Sci U S A 2006; 103: 14678-14683.

[17] Pasternak RC, Criqui MH, Benjamin EJ, Fowkes FG, Isselbacher EM, McCullough PA, Wolf PA, Zheng ZJ and American Heart A. Atherosclerotic Vascular Disease Conference: Writing Group I: epidemiology. Circulation 2004; 109: 2605-2612.

[18] Halliday A, Harrison M, Hayter E, Kong X, Mansfield A, Marro J, Pan H, Peto R, Potter J, Rahimi K, Rau A, Robertson S, Streifler J, Thomas D; Asymptomatic Carotid Surgery Trial (ACST). 10-year stroke prevention after successful carotid endarterectomy for asymptomatic stenosis (ACST-1): a multicentre randomised trial. Lancet 2010; 376: 1074-1084.

[19] Redgrave JN, Lovett JK, Gallagher PJ and Rothwell PM. Histological assessment of 526 symptomatic carotid plaques in relation to the nature and timing of ischemic symptoms: the Oxford plaque study. Circulation 2006; 113: 2320-2328.

[20] Lusis AJ. Atherosclerosis. Nature 2000; 407: 233-241.

[21] Ambrose JA, Winters SL, Stern A, Eng A, Teichholz LE, Gorlin R and Fuster V. Angiographic morphology and the pathogenesis of unstable angina pectoris. J Am Coll Cardiol 1985; 5: 609-616.

[22] Alexander JJ, Moawad J and Super D. Outcome analysis of carotid artery occlusion. Vasc Endovascular Surg 2007; 41: 409-416.

[23] Barrett JF and Keat N. Artifacts in CT: recognition and avoidance. Radiographics 2004; 24: 1679-1691.